6 July 2001

ELSEVIER

Chemical Physics Letters 342 (2001) 75–84

CHEMICAL PHYSICS LETTERS

www.elsevier.com/locate/cplett

Photodissociation spectra of transition metal sulfides: spin–orbit structure in charge transfer bands of FeS^+ and NiS^+

John Husband, Fernando Aguirre, Christopher J. Thompson, Ricardo B. Metz *

Department of Chemistry, University of Massachusetts, Amherst, MA 01003-9336, USA

Received 23 March 2001; in final form 18 April 2001

Abstract

Photofragment spectra of FeS^+ and NiS^+ are reported. Analysis of the FeS^+ spectrum reveals it to arise from a $^6\Pi \leftarrow {}^6\Sigma$ charge-transfer transition, and gives the vibrational frequency, $\omega'_e = 295\ cm^{-1}$, and spin–orbit constant, $|A| = 125\ cm^{-1}$, in the $^6\Pi$ state. The onset of the NiS^+ spectrum appears to occur in the middle of a vibrational progression, thus giving a precise measurement of the Ni^+–S bond strength, $D_0(Ni^+–S) = 238 \pm 4\ kJ\ mol^{-1}$. Analysis of the spectrum for vibrational and spin–orbit structure leads to a tentative assignment of a $^4\Delta$ ground state and suggests the spectrum is composed of overlapping transitions to two near-degenerate excited electronic states, most likely a $^4\Pi$ and $^4\Phi$ pair. © 2001 Elsevier Science B.V. All rights reserved.

1. Introduction

Sulfur ligation is prevalent throughout bioinorganic chemistry. Of the 10 essential transition metals found in biological systems, seven, including iron and nickel, are commonly coordinated to sulfur [1]. Indeed, one of the most striking structural motifs found in metalloenzymes is the thiocubane clusters of ferredoxins: the cubic arrangement of alternating iron and sulfur atoms. Metal–sulfur interactions also play an important role in industrial systems. Most notably, molybdenum and tungsten sulfides serve as catalysts in the hydrotreating of fossil fuels, removing nitrogen, oxygen, sulfur and heavy metals from the feedstock prior to refining [2].

While the above examples concern metal sulfides in the condensed phase, the focus of this paper is on the cations of bare, gas-phase, transition-metal sulfides, specifically FeS^+ and NiS^+. Studying these bare sulfides gives us an opportunity to gain insight into the intrinsic properties of the metal-sulfur bond in an environment uncomplicated by additional interactions. These species thus serve as useful models for more complicated systems. For example, gas-phase FeO^+ can convert methane to methanol and has been suggested to be a model for the active site in soluble methane monooxygenase [3]. Like FeO^+, FeS^+ and NiS^+ show interesting chemistry. Freiser and co-workers [4] studied the reactions of MS^+ (M = Fe, Co, Ni) with a variety of small alkanes and showed them to proceed via an excited H_2S–M^+-alkene complex to give products resulting from elimination of either an alkene or H_2S. An additional channel leading to M^+ is also seen. For FeS^+ and CoS^+ the major elimination channel is loss of H_2S, while

* Corresponding author. Fax: +1-413-545-4490.
E-mail address: rbmetz@chemistry.umass.edu (R.B. Metz).

0009-2614/01/$ - see front matter © 2001 Elsevier Science B.V. All rights reserved.
PII: S0009-2614(01)00553-X

NiS^+ gives a more even distribution of alkene- and H_2S-loss products. Following the elimination of H_2S, the M^+-alkene complex can retain sufficient excess energy to undergo further rearrangement with the accompanying loss of small hydrocarbons such as CH_4 or C_2H_4. Finally, for alkanes larger than ethane, products resulting from the direct insertion of the metal sulfide into a C–C bond were also seen. In a parallel series of experiments [5], Freiser and co-workers measured the photofragment spectra of M^+–S, M = Fe, Co, Ni. From the observed photodissociation onsets they assigned upper bounds to the M^+–S bonds of 272 ± 20, 260 ± 20 and 250 ± 20 kJ mol^{-1}, respectively. The resolution of these early studies was limited to 10 nm by the lamp-monochromator combination used in their experiments. In the course of a recent series of mass-spectrometric studies focusing on FeS_2^+, Schröder et al. were able to measure the bond energy for Fe^+–S to noteworthy precision in two independent experiments [6]. Such is their confidence in the measured value $D_0(Fe^+–S) = 297 \pm 4$ kJ mol^{-1} that they offer this number as a benchmark for future calculations of molecules containing transition metals. Using the B3LYP/6-311+G* level of theory they calculate $D_0(Fe^+–S) = 299$ kJ mol^{-1}, in excellent agreement with their measured value. Both the measured and calculated values of Schröder et al. are in slight disagreement with the earlier spectroscopic measurement of the Fe^+–S bond strength by Freiser and co-workers.

The large number of electronic states and the high spin and/or orbital angular momentum quantum numbers associated with these molecules complicates the electronic spectra of the diatomic metal sulfides. In the spectra discussed in this Letter, a single photon is used to excite the MS^+ molecule to a state from which it can dissociate to M^+ and S. The resolution of the spectrum, and hence the amount of information we can obtain from it, is typically determined by the predissociation lifetime of the molecule rather than the linewidth of our lasers. As we have previously demonstrated with FeO^+ [7], and now again with the results reported here, excellent spectroscopic information can be obtained from photofragment spectra of predissociative states of metal-containing diatomics. Since these are the only optical spectra of FeS^+ and NiS^+ other than the much lower resolution studies of Freiser and co-workers [5], we are able to resolve the discrepancy between the measured dissociation energies for FeS^+ and report an improved dissociation energy for NiS^+.

2. Experimental approach

The photodissociation experiments were performed in a home built dual time-of-flight mass spectrometer described in detail elsewhere [7]. MS^+ ions (M = Fe, Ni) produced in a laser-ablation source [8,9] undergo expansion into vacuum, are skimmed into a differentially pumped chamber and enter the extraction region of a Wiley–McLaren time-of-flight mass spectrometer [10]. Positive ions formed in the source are temporally separated in a field-free flight tube and enter a reflectron positioned at its end. Photodissociation of the desired ion is initiated at the turning point of the reflectron using the unfocused output of a Nd:YAG-pumped dye laser. Fragment ions are identified from their characteristic flight times through a field-free region to the detector. The photofragment spectrum is obtained by monitoring the yield of the M^+ fragment ion as a function of laser wavelength and normalizing to parent ion signal and laser power.

For these studies methanethiol (methyl mercaptan) (99.5+% Sigma-Aldrich) was used to make the metal sulfides:

$$M^+ + CH_3SH \rightarrow MS^+ + CH_4, \quad M = Fe, Ni. \tag{1}$$

Typically, gas mixtures of 1–2% CH_3SH, 10% N_2 in He were used with backing pressures of 3 atm. Including N_2 in the mix has been shown [7] to be an effective method of producing vibrationally cold parent ions in this source. Similar conditions led to the production of FeO^+ [7] with a rotational temperature of 8 K. High purity rods (Fe, 99.98% Sigma-Aldrich; Ni, 99+% Strem) served as the source for metal ions.

Light for the FeS^+ study was generated using the frequency-doubled output of the dye laser,

pumped by the 532 nm second harmonic of the Nd:YAG. The longer wavelengths used in the NiS^+ investigation were generated using the fundamental output of the dye laser pumped with the 355 nm third harmonic of the Nd:YAG. Linewidths are <0.1 cm^{-1} for the dye fundamental and <0.2 cm^{-1} for the frequency-doubled output. In both cases, dissociation at a peak was found to be linear with laser fluences up to $\sim$15 mJ cm^{-2}. To minimize contributions from two-photon processes, laser fluences were kept below 10 mJ cm^{-2}.

3. Results and discussion

3.1. FeS^+

Photodissociation of $^{56}Fe^{32}S^+$ between 28 000 and 33 000 cm^{-1} gives rise to the spectrum shown in Fig. 1a. As seen in the figure, the spectrum consists of some 30 peaks and reaches a maximum near 30 500 cm^{-1} before falling off again at higher energies. Individual peaks are $\sim$110 cm^{-1} wide, due to lifetime broadening. As the peaks are only $\sim$140 cm^{-1} apart, they partially merge, giving an almost symmetrical envelope with a width of 2000 cm^{-1}. In an earlier study, Freiser and coworkers [5] recorded the photofragment spectrum of FeS^+ between 240 and 460 nm with 10 nm ($\sim$1000 cm^{-1} at 300 nm) resolution. They showed the spectrum to be dominated by a single intense peak centered at 320 nm (31 200 cm^{-1}) with a width of 30 nm ($\sim$3000 cm^{-1}). This peak clearly corresponds to the envelope of peaks seen in our study. The presence of a low-intensity tail extending to 440 nm led Freiser and co-workers to assign a threshold at 440 nm, giving an upper limit value $D_0(Fe^+–S) \leqslant 272 \pm 20$ kJ mol^{-1}. Our results show only extremely low levels of background dissociation at wavelengths longer than 360 nm implying that the tail observed in Freiser's study is likely due to electronically excited ions. This is supported by the recent investigation of the $Fe^+ - S$ bond strength by Schröder et al. [6] who find $D_0(Fe^+–S) = 297 \pm 4$ kJ mol^{-1} (24 800 $\pm$ 300 cm^{-1}) based on ion–molecule reactions.

The mass-spectrometric studies of Schröder et al. show the Fe^+–S bond strength lies somewhat below the apparent onset at $\sim$28 000 cm^{-1} shown in Fig. 1a. This implies that our observed onset is spectroscopic, rather than thermodynamic in nature. Thus, near 28 000 cm^{-1}, FeS^+ either does not absorb or is excited to a state from which it cannot easily dissociate. However, at energies this far above the dissociation limit we would expect a sufficiently high density of states such that

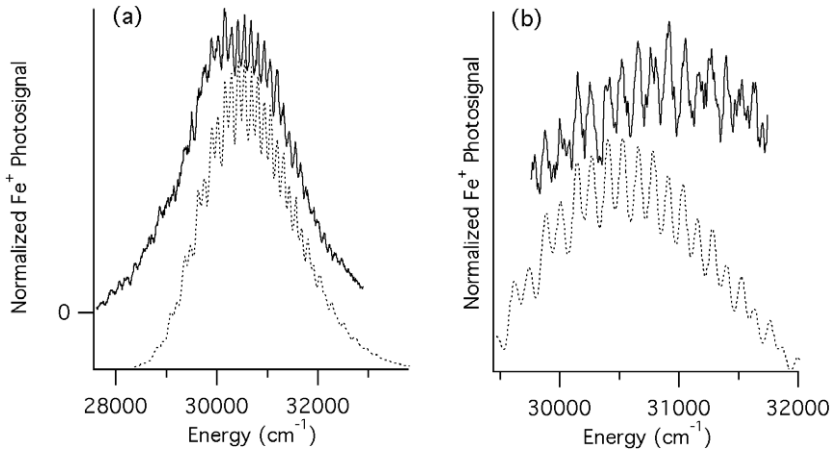

Fig. 1. Measured (solid lines) and simulated (dashed lines) photofragment spectra of: (a) $^{56}Fe^{32}S^+$ and (b) $^{56}Fe^{34}S^+$. The intensity of the measured peaks in panel (b) are biased in favor of those not saturated at high laser fluences, see text. In each case the simulations are offset from the measured data to facilitate comparison. The spectra consist of six overlapping vibrational progressions each offset by approximately the separation between adjacent peaks.

absorption would lead to dissociation. We therefore conclude that limited photofragment signal below ~28 000 cm^{-1} and above 32 500 cm^{-1} arises from lack of absorption in FeS^+.

In addition to recording the spectrum of the major isotopomer $^{56}Fe^{32}S^+$, data was also collected for $^{56}Fe^{34}S^+$, which has a natural abundance of 4.2%. Since the experiment is performed in a mass-spectrometer, changing to the heavier isotopomer simply entails delaying the dissociation laser firing time. The $^{56}Fe^{34}S^+$ spectrum is shown in Fig. 1b. Two points should be noted, first, because of the low natural abundance of $^{56}Fe^{34}S^+$, its spectrum was recorded only over the wavelength region in which it absorbs strongly. Second, in order to increase signal levels, laser fluences were increased to a point (20 mJ cm^{-2}) such that dissociation was somewhat less than linear with laser power in sections of the region covered. Therefore, although the peak positions are accurately given in the figure, the normalized intensities are skewed in favor of those peaks not saturated at the higher laser fluences.

We first attempted to model the spectrum as a single vibrational progression, calculating Franck–Condon factors using Morse potentials for the ground and excited electronic states. FeS^+ ground-state parameters were fixed at the values calculated by Schröder et al. [6] at the B3LYP/6-311+G* level of theory. These values, which are given in Table 1, were chosen since no experimental measurements have been reported for this molecule. Additionally, because under similar conditions as those used for FeS^+ production the source has been shown [7] to produce vibrationally cold molecules nearly exclusively, contributions from vibrationally excited molecules were ignored. The resulting simulations did not come close to approximating the observed spectrum. Neither the number of observed peaks, nor the shape and width of the overall envelope, were captured with any physically reasonable change in bond length. Also, the spacing between peaks leads to an unrealistically low upper-state vibrational frequency of $\omega'_e = 142$ cm^{-1}, far lower than the calculated $\omega''_e = 463$ cm^{-1}. For comparison, Brucat and co-workers have measured vibrational frequencies of $\omega'_e = 120, 164$ and 175 cm^{-1} in three excited electronic states of $CoAr^+$ [11]. It is unlikely that the vibrational frequency in covalently bound FeS^+ would be lower that in $CoAr^+$ for which the bonding is purely electrostatic.

Table 1
Molecular parameters for FeS^+

Constant	$X^6\Sigma^+$	$^6\Pi$
T_0 (cm^{-1})		28 500 ± 300
ω_e (cm^{-1})	463[a]	295 ± 3
$\omega_e x_e$ (cm^{-1})	2.14[b]	2.5 ± 0.1
r_e (Å)	2.06[a]	2.28 ± 0.02
$\|A\|$ (cm^{-1})		125 ± 5
τ (fs)		45 ± 5

[a] Calculated by Schröder et al. [6] at the B3LYP/6-311+G* level of theory.
[b] Value calculated from reported ω_e and D_0.

The failure of these simulations implies that the sequence of peaks is not a simple vibrational progression. The most likely explanation is that the progression contains a multiplet component, with the spacing between the multiplet sub-bands sufficiently large to be observed at the experimental resolution. This we find to be the case. Schröder et al. [6] calculate a $^6\Sigma^+$ ground state for FeS^+. This agrees with $^6\Sigma^+$ ground-state assignments for both isovalent FeO^+ [7] and isolectronic neutral MnS [12]. From a $^6\Sigma^+$ ground state allowed transitions can occur to either another $^6\Sigma^+$ state or a $^6\Pi$ state. Since a $^6\Sigma^+ \leftarrow {}^6\Sigma^+$ transition would show no first-order spin–orbit coupling and second-order spin–orbit coupling would not be expected to be sufficiently large [13] to affect the observed spectrum, we turn to a $^6\Pi \leftarrow {}^6\Sigma^+$ transition. With near case (a) coupling, a $^6\Pi \leftarrow {}^6\Sigma^+$ transition causes each vibrational peak to be split into six components corresponding to the six $\Delta\Omega = \Delta\Lambda = 1$ sub-bands [14]. The simulations shown in Fig. 1 were calculated with the upper-state vibrational frequency equal to the spacing between every other peak in the observed spectrum, and the spacing between adjacent peaks corresponding to the spin–orbit splitting. The observed spectrum thus consists of six overlapping vibrational progressions each offset by approximately half the vibrational frequency. This arrangement of peaks captures both the near flat-topping of the observed envelope and the pattern of near doublets found on the low-energy

side of the spectra. We also simulate the spectrum of the $^{56}Fe^{34}S^+$ isotopomer, using the same potential as for $^{56}Fe^{32}S^+$. The excellent agreement between the observed and simulated spectra for $^{56}Fe^{34}S^+$ confirms our assignments.

The best-fit values from the Franck–Condon analysis are summarized in Table 1 along with the ground-state parameters calculated by Schröder et al. [6]. The large predicted change in bond length of $\Delta r = 11\%$ and the observation of a lower vibrational frequency in the upper state than the ground state is consistent with a charge-transfer transition [15]. This idea is further supported by the strong intensity of the observed band.

Before we discuss these results in detail, it is useful to refer to a relatively simple molecular orbital picture used by several authors [15–18] to help describe the electronic structure of diatomic molecules containing a first-row transition metal. For neutral metal sulfides the lowest-lying valence orbitals are the 10σ and 4π orbitals, which are predominately ligand in character. Above these, and very closely grouped in energy, lie the nonbonding 11σ and 1δ orbitals and weakly antibonding 5π and 12σ orbitals, all of which retain metal character. At higher energies are the 6π and 13σ orbitals derived from the metal 4p orbitals. The order remains the same for the corresponding cations, but, because of the charge on the metal, the metal orbitals are lowered in energy relative to the sulfur 3p orbitals. Thus, the lower orbitals gain metal character while the higher-energy orbitals show an increased contribution from the ligand. Using this description, the $X^6\Sigma^+$ state of FeS^+ has an orbital occupancy of (core) $(10\sigma)^2(4\pi)^4(1\delta)^2(11\sigma)^1(5\pi)^2$. A feel for the relative separation of these orbitals can be gleaned from a recent study of CoO^+ performed by Brucat and co-workers [19] who observe the $3\pi \rightarrow 10\sigma$ charge transfer transition in CoO^+ near 17 000 cm^{-1}. This would correspond to a $4\pi \rightarrow 12\sigma$ transition in the sulfide. Therefore, at the higher energies of the present study and based on the strong evidence supporting a charge-transfer transition, the upper $^6\Pi$ state is likely derived from either a $10\sigma \rightarrow 6\pi$, or a $4\pi \rightarrow 13\sigma$ transition. These transitions move electron density from a predominately S 3p orbital to a predominately Fe^+ 4p orbital. Although transitions to the 4p orbital in bare Fe^+ occur at energies beyond those used in this study [20] (the $3d^64s^1(^6D) \rightarrow 3d^64p^1(^6D)$ transition occurs at 38 459 cm^{-1}), interactions with the ligand lower the transition energy [21,22].

Lefebvre-Brion and Field provide a means of roughly estimating the spin–orbit constant in FeS^+ using atomic parameters [13]. Assuming the spin–orbit interactions arise from a single electron in the 6π (Fe 4p) orbital, then $A\Lambda\Sigma \approx \zeta_{4p}/2$. Therefore, for a $^6\Pi$ state, with $\Sigma = 5/2$ and $\Lambda = 1$, $A \approx \zeta_{4p}/5$. Since $\zeta_{4p} = 405$ cm^{-1} for $Fe^+(3d^64p^1)$ and 545 cm^{-1} for $Fe^+(3d^54s^14p^1)$, [23] $A \approx 81$ or 109 cm^{-1}. A similar result ($A \approx 76$ cm^{-1}) is obtained if we assume the $^6\Pi$ state is derived from a single electron in the 4π (S 3p) orbital. The observed value of $A = 125$ cm^{-1} is consistent with these rough estimates. This is in fact $|A|$ as the simulation is only sensitive to the magnitude of the spin–orbit constant. In order to simulate the observed spectrum, the vibrational peak intensities from a Franck–Condon analysis are convoluted with a Lorentzian [13] with a width of 110 cm^{-1}. At the rotational temperature of the ion beam, this is much broader than any rotational structure and the width is thus due to lifetime broadening. The lifetime of the excited state is then 45 fs. The spectral broadening, and hence lifetime, is essentially uniform across the vibrational progression. This is in stark contrast to the predissociative $^6\Sigma^+ \leftarrow {}^6\Sigma^+$ transition observed in FeO^+ near 350 nm, for which the lifetime in the $v' = 1$ state is 140 fs compared to 3500 fs in the $v' = 0$ state [7].

The shown simulation has the $0 \leftarrow 0$ transition at 28 500 cm^{-1} for the lowest spin–orbit state in $^{56}Fe^{32}S^+$. This assignment is good to ± 1 vibrational peak, leading to an uncertainty of 300 cm^{-1}. Shifting the position of the $0 \leftarrow 0$ transition by one vibrational peak requires correcting the quoted vibrational constant by an amount equal to the anharmonicity. For example, changing the assignment of the $0 \leftarrow 0$ transition to the $1 \leftarrow 0$ transition would change the vibrational constant to $295 + 2.5$ $cm^{-1} = 298$ cm^{-1}. Using the optimized values of ω'_e and $\omega'_e x'_e$, we can extrapolate to find the dissociation energy of the excited state. Shifting the assignment of the $0 \leftarrow 0$ transition does not affect this extrapolation. The predicted

value is $D_0 = 8500 \pm 1500$ cm^{-1}. This value, together with the measured [6] ground-state dissociation energy of $24\,800 \pm 300$ cm^{-1}, and the $0 \leftarrow 0$ transition at 28 500 cm^{-1} allows us to predict the energy separation between ground-state fragments and those which adiabatically correlate to the predissociative state. This separation is $12\,200 \pm 1600$ cm^{-1}. The only combination of atomic states which falls within this energy range [20] and can be combined to form a $^6\Pi$ state is $Fe^+(^4P_J)$ ($E^* = 13\,474$ cm^{-1} for $J = 7/2$) + $S(^3P_J)$. Fig. 2 shows schematic potential curves for the ground and observed excited state of FeS^+.

The match between the observed and simulated spectra is poorest on the low energy side. For the simulation it was assumed that FeS^+ was produced vibrationally cold. Since contributions from hot bands would have the largest effect at low energy, the neglect of these bands may well explain the small disparity between the observed and simulated spectra.

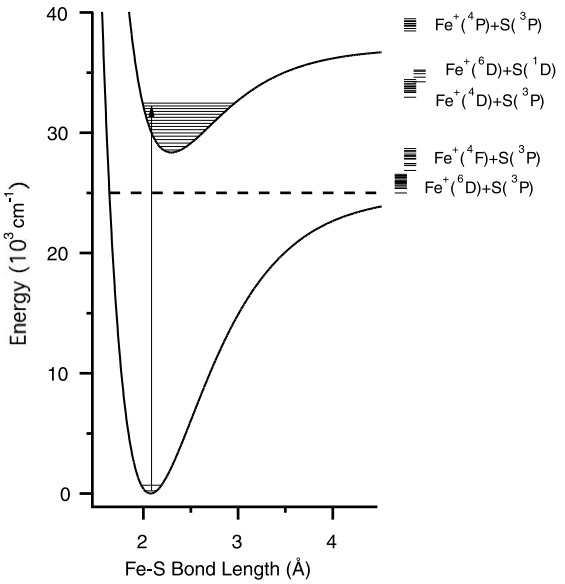

Fig. 2. Schematic potential curves for FeS^+. The ground state potential is based on B3LYP/6-311+G* calculations; excited state potentials are based on observed transitions. For clarity, only the lowest spin–orbit state of the $^6\Pi$ excited state is included. Asymptotic energy levels leading to sextet states are shown.

3.2. NiS^+

Despite the underlying complexity, the photofragment spectrum of FeS^+ is quite regular in appearance. The same cannot be said for NiS^+. As seen in Fig. 3, the spectrum between 20 000 and 23 000 cm^{-1} consists of 12 major peaks falling off in intensity at higher energies. Each of the 12 peaks is composed of a number of partially resolved features. Interestingly, the spectrum shown here differs from the low-resolution spectrum previously reported by Freiser and co-workers [5], where we see an increase in intensity at lower energies they see a decrease. Their spectrum shows a large peak between 400 and 450 nm (25 000 and 22 000 cm^{-1}) with a maximum intensity at 420 nm. A low-intensity tail extends from this peak to 480 nm (20 800 cm^{-1}). Even at the 10 nm resolution (600 cm^{-1} at 400 nm) of their study, the peak is not smooth, hinting at hidden structure. From the threshold at 480 nm they assigned $D_0(Ni^+ - S) \leqslant 250 \pm 20$ kJ mol^{-1}.

Although the appearances of the spectra differ, we are in agreement with the assigned threshold. Our results show a threshold at 19 900 cm^{-1}, imposing a strict upper limit to the Ni^+–S bond strength of 238 ± 4 kJ mol^{-1}. The rather conservative error bars correspond to ±1 major peak. In this case, we contend that the observed onset is governed by the thermodynamics of the system

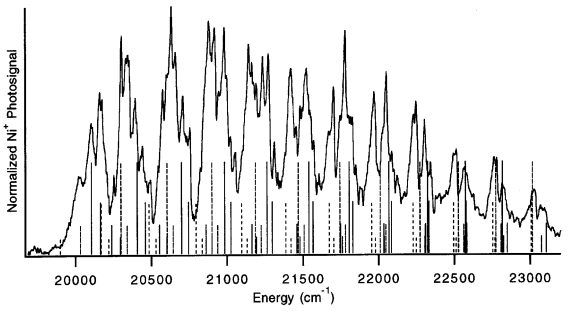

Fig. 3. Photofragment spectrum of $^{58}Ni^{32}S^+$. The onset at 19 900 cm^{-1} imposes a strict upper limit to the Ni^+–S bond strength of $D_0(Ni^+–S) = 238 \pm 4$ kJ mol^{-1}. Also shown are stick spectra assigning peak positions to vibrational and spin–orbit structure using parameters given in Table 2. Transitions to state 1 are shown with a solid line, those to state 2 are dashed. Stick heights do not reflect transition intensities. Rather, the longest sticks correspond to $\Omega_{i=0}$, and the shortest to $\Omega_{i=3}$.

and that the assigned upper limit lies at, or very close to, the actual Ni^+–S bond strength. We make this assertion based on the appearance of the measured spectrum. The spectrum has a maximum at the third major peak, followed by a long, gradual decrease in peak intensities at higher energies. The two peaks to the low-energy side of the maximum each have >70% of its intensity. This behavior is not reproduced by Franck–Condon simulations in which the first-observed peak corresponds to a $0 \leftarrow 0$ transition. Simulations giving rise to long progressions are far more symmetrical with a much more gradual build up in intensity. These simulations suggest that the first-observed peak corresponds to the $4 \leftarrow 0$ band, and that transitions to lower vibrational levels would be expected to have appreciable intensity but are missing from the observed spectrum. Therefore, we conclude that photons below 19900 cm^{-1} have insufficient energy to dissociate NiS^+, giving $D_0(Ni^+–S) = 238 \pm 4$ kJ mol^{-1}. To test this conclusion, $D_0(Ni^+–S)$ was calculated at the B3LYP/6-311+G* level of theory using GAUSSIAN 98 [24]. Similar, relatively simple, 'black box' calculations have been shown to give bond energies accurate to ± 15 kJ mol^{-1} in a series of iron-containing molecules [25]. We calculate $D_0(Ni^+–S) = 225$ kJ mol^{-1}, which considering the accuracy of the calculation, agrees with our measured value.

As a result of the short lifetime in the excited state only broad structural features are observed in the NiS^+ spectrum. At the ~8 K rotational temperature [7] of the ions in the molecular beam, rotations do not contribute to the observed structure as the rotational envelope is much narrower than even the sharpest feature in the spectrum. This effectively rules out a rotational analysis. In order to proceed further, we make use of the ground-state assignment from our density functional calculation. At the B3LYP/6-311+G* level of theory the ground-state is found to be one of near degenerate pair of $^4\Sigma$ and $^4\Delta$ states. Therefore, since a higher level of theory will be needed to determine which of these states is the true ground state, in our subsequent analysis, we consider both the $^4\Sigma$ and the $^4\Delta$ state as possible candidates. The isoelectronic neutral CoS radical also has low-lying $^4\Sigma$ and $^4\Delta$ states. In this case, the more sophisticated calculations [17,26] predict a $^4\Delta$ ground state, with the $A^4\Sigma$ state just 1770 cm^{-1} higher [17].

Since a rotational analysis is not possible, we have to content ourselves with assigning observed peaks to vibrational and spin–orbit structure. To a first approximation, in Hund's case (a) coupling the energy for an electronic transition between vibrational and spin–orbit levels may be written as: [14]

$$\Delta T(v', \Omega', v''\Omega'') = T_0 + \omega'_{\Omega'}(v') - \omega'_{\Omega'}x'_{\Omega'}(v')(v'+1) + i(\mathrm{A}' \cdot \Lambda' - \mathrm{A}'' \cdot \Lambda''), \quad (2)$$

where i takes integer values reflecting the multiplicity of the transition: in this case $i = 0, 1, 2, 3$. T_0 is given with respect to the transition from the lowest energy Ω level, rather than from the multiplet average energy. Again, here we assume that our ions are vibrationally cold ($v'' = 0$). We do not, however, assume that all the ions are in the lowest spin–orbit state. While we can effectively quench excited vibrational states, reaction (1) is sufficiently exothermic to populate excited spin–orbit states of NiS^+ that we would not expect to efficiently cool with simple closed-shell collision partners such as helium or N_2.

As given by Eq. (2), transitions from a quartet state will give four sub-bands corresponding to $\Delta\Lambda = \Delta\Omega$ transitions. The exception is a $^4\Sigma \leftarrow {}^4\Sigma$ transition which is unsplit to first-order. Patterns of four peaks within the major peaks can readily be picked out in the observed spectrum. Simulations aimed at capturing the peak positions were then attempted based on Eq. (2). These simulations are most sensitive to the difference $(\mathrm{A}' \cdot \Lambda')$ $(\mathrm{A}'' \cdot \Lambda'')$ which was thus used as a single parameter, Δsos. This reproduces about half of the structure in the spectrum. To fit the remaining structure, we reuse the same expression with new parameters, implying the observed spectrum is composed of transitions to two distinct excited electronic states. If we first consider a single $X^4\Sigma$ state, then both of these excited states must be $^4\Pi$ states, since a $^4\Sigma \leftarrow {}^4\Sigma$ transition would not fit the observed structure. However, we feel it is

unlikely that transitions to two $^4\Pi$ states could overlap so strongly without severely perturbing each other. Since the simulations of the peak positions show no evidence of such a perturbation, we are led to favor the assignment of a $^4\Delta$ ground state. From a $^4\Delta$ state optical transitions can occur to $^4\Pi$, $^4\Delta$ or $^4\Phi$ excited states. It is common in metal systems of this type to find near-degenerate electronic states differing by two orbital angular momentum units. For example, Brucat and co-workers have observed transitions from the $X^5\Delta_4$ state of CoO^+ to the $B^5\Phi_5$ and $C^5\Pi_3$ states at 16 713 and 17 588 cm^{-1}, respectively [27]. It is appealing, although far from rigorous, to think of the two states accessed in this study as a pair of $^4\Pi$ and $^4\Phi$ states. Our simulations show vibrational progressions of 12 peaks above the dissociation energy. The lengths of these progressions are indicative of large changes in bond length upon electronic excitation consistent with charge transfer transitions.

The constants used for the simulation of the peak positions are given in Table 2. Simulations were initially attempted with a single vibrational constant for each of the two excited states. These were not successful and we quickly moved to a vibrational constant for each sub-band. This has previously been reported in, for example, the $^6\Pi \leftarrow X^6\Delta$ transition in FeCl [28]. The use of individual vibrational constants for each Ω level correctly captures the transition from multi-component peaks in the low energy portion of the spectrum to near-doublets found at higher energies. A single anharmonicity constant is used for all Ω levels of each electronic state, as the slight improvement in the fit obtained by using a separate value for each Ω level does not justify the introduction of additional parameters. Since the first observed band for each state is not the $0 \leftarrow 0$ band it is convenient to recast Eq. (2) to give:

$$\Delta T(v', \Omega', v''\Omega'') = T_n + \omega'_{\Omega'_n}(v'_n) - \omega'_{\Omega'}x'_{\Omega'}(v'_n) \times (v'_n + 1) + \mathrm{i}(\Delta\mathrm{sos}), \quad (3)$$

where n is the vibrational quantum number for the first observed peak (which has $v'_n = 0$), and

$$v'_n = v' - n, \quad (4)$$

$$T_n = T_0 + \omega'_{\Omega'} \cdot n - \omega'_{\Omega'}x'_{\Omega'} \cdot (n^2 + n), \quad (5)$$

$$\omega'_{\Omega'_n} = \omega'_{\Omega'} - 2n \cdot \omega'_{\Omega'}x'_{\Omega'}. \quad (6)$$

Table 2
Results of the peak-position analysis for NiS^+

Constant	State 1[a]	State 2[a]
T_n (cm^{-1})	20 105	20 300
ω_{Ω_n}(cm^{-1}) $\Omega_{i=0}$[b]	305	310
$\Omega_{i=1}$	299	322
$\Omega_{i=2}$	321	316
$\Omega_{i=3}$	312	325
$\omega_e x_e$(cm^{-1})	3.1	3.5
Δsos(cm^{-1})[c]	60	−130

[a] Without readily assignable rotational structure we are unable to determine the symmetry of the excited states and therefore label them simply States 1 and 2.
[b] Ω states labeled by index i, see Eq. (2). T_n and ω_{Ω_n} are defined in Eqs. (4) and (5) in the text.
[c] $\Delta\mathrm{sos} = (\mathrm{A}' \cdot \Lambda')(\mathrm{A}'' \cdot \Lambda'')$.

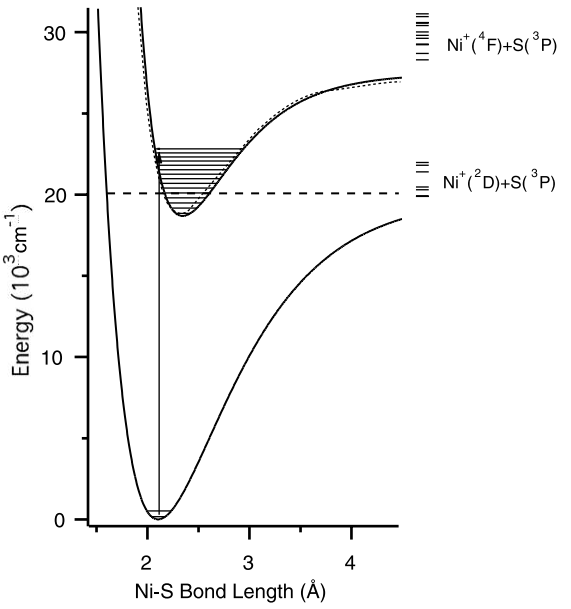

Fig. 4. Schematic potential curves for NiS^+. The ground state potential is based on B3LYP/6-311+G* calculations; excited state potentials are based on observed transitions, assuming the first observed peak in the spectrum is to $v = 4$ in each excited state. The potential for excited state 1 and its vibrational levels are shown with a solid line, while the potential for state 2 is dashed. For clarity, only $\Omega_{i=0}$ spin–orbit states are included. Asymptotic energy levels leading to quartet states are indicated.

Solving Eq (3) for the maximum value of ΔT gives the adiabatic dissociation energy of the two excited states. This does not require knowledge of the absolute vibrational numbering. The difference between the calculated ΔT_{max} for each state and the measured $D_0(Ni^+–S)$ is 7500 ± 1500 cm^{-1}, implying that the excited states both correlate to $Ni^+(^4F_{9/2}) + S(^3P_J)$ at 8394–8967 cm^{-1} [20]. Fig. 4 shows schematic potential curves for the ground and observed excited states of NiS^+.

Before closing this section, another possible explanation for the large number of peaks in the observed spectrum should be mentioned. Both our B3LYP calculations and the results for CoS [17,26] suggest that NiS^+ has low-lying $^4\Delta$ and $^4\Sigma$ states. Transitions from these states to a common $^4\Pi$ upper state would give a sufficient number of peaks to simulate the observed spectrum. However, although the vibrational constants given for the two states in Table 2 are similar, they are sufficiently different to make it seem likely that more than one excited state is involved.

4. Conclusions

Photofragmentation spectra are reported for FeS^+ and NiS^+. The FeS^+ spectrum, which is recorded at energies well above the dissociation energy, reflects the absorption properties of this molecule. The spectrum is found to consist of a long vibrational progression in the excited state which is split into six sub-bands by spin–orbit coupling consistent with a $^6\Pi \leftarrow X^6\Sigma^+$ transition. Calculations of the Franck–Condon overlap have been performed to reproduce the vibrational and spin–orbit structure. These simulations show that electronic excitation is accompanied by a large change in bond length (11%) characteristic of a charge-transfer transition. In terms of a simple single configuration molecular orbital picture, this most likely corresponds to either a $10\sigma \rightarrow 6\pi$ or $4\pi \rightarrow 13\sigma$ transition. Calculated excited-state parameters are $\omega_e = 295$ cm^{-1} and $|A| = 125$ cm^{-1}. The observed spectrum shows lifetime broadening corresponding to a lifetime in the excited state of 45 fs.

The NiS^+ spectrum is recorded at energies just above the dissociation energy. The observed onset at 19900 cm^{-1} imposes a strict upper limit to the Ni^+–S bond strength of $D_0(Ni^+–S) \leqslant 238 \pm 4$ kJ mol^{-1}. However, since the onset appears to occur in the middle of a vibrational progression it is likely that this threshold gives more than an upper limit and that $D_0(Ni^+–S) = 238 \pm 4$ kJ mol^{-1}. This is supported by B3LYP calculations. At the B3LYP/6-311+G* level of theory, the NiS^+ ground state is predicted to be one of a near degenerate pair of $^4\Sigma$ and $^4\Delta$ states. No rigorous analysis of the spectrum has been completed, but simulations of the peak positions have been performed to gain insight into how such a spectrum might arise. These simulations favor the assignment of a $^4\Delta$ ground state and suggest that two near-degenerate electronic states are accessed in the energy region of this study. Allowed transitions from a $^4\Delta$ ground state can occur to $^4\Pi$,$^4\Delta$, or $^4\Phi$ states. In each case a pattern of four sub-bands would be expected, such sub-bands are observed in the spectrum. With no obvious rotational structure to aid in the analysis we are unable to distinguish between the three possible states. Vibrational constants are found to be slightly different for each Ω level, but are close to 300 cm^{-1} in both states. The length of the vibrational progression suggests a charge transfer transition with an accompanying large change in bond length.

Acknowledgements

Support of this work by a National Science Foundation Faculty Early Career Development Award (NSF CHE 9875220) is gratefully acknowledged.

References

[1] E.I. Stiefel, K. Matsumoto (Eds.), Transition Metal Sulfur Chemistry, Number 653, ACS Symposium Series, American Chemical Society, Washington, DC, 1996.
[2] T. Weber, R. Prins, R.A. van Santen (Eds.), Transition Metal Sulphides Chemistry and Catalysis, vol. 60, NATO ASI Series 3. High Technology, Kluwer Academic Publishers, Dordrecht, 1998.
[3] K. Yoshizawa, J. Biol. Inorg. Chem. 3 (1998) 318.
[4] T.C. Jackson, T.J. Carlin, B.S. Freiser, Int. J. Mass Spectrom. Ion Proc. 72 (1986) 169.

[5] R.L. Hettich, T.C. Jackson, E.M. Stanko, B.S. Freiser, J. Am. Chem. Soc. 108 (1986) 5086.
[6] D. Schröder, I. Kretzschmar, H. Schwarz, C. Rue, P.B. Armentrout, Inorg. Chem. 38 (1999) 3474.
[7] J. Husband, F. Aguirre, P. Ferguson, R.B. Metz, J. Chem. Phys 111 (1999) 1433.
[8] T.G. Dietz, M.A. Duncan, D.E. Powers, R.E. Smalley, J. Chem. Phys. 74 (1981) 6511.
[9] P.J. Brucat, L.-S. Zheng, C.L. Pettiette, S. Yang, R.E. Smalley, J. Chem. Phys. 84 (1986) 3078.
[10] W.C. Wiley, I.H. McLaren, Rev. Sci. Instr. 26 (1955) 1150.
[11] D. Lessen, R.L. Asher, P. Brucat, Int. J. Mass Spec. Ion. Proc. 102 (1990) 331.
[12] M. Douay, B. Pinchemel, C. Dufour, Can. J. Phys. 63 (1985) 1380.
[13] H. Lefebvre-Brion, R. Field, Perturbations in the Spectra of Diatomic Molecules, Academic Press, London, 1986.
[14] G. Herzberg, Spectra of Diatomic Molecules, Van Nostrand Reinhold, New York, 1950.
[15] A.J. Merer, Ann. Rev. Phys. Chem. 40 (1989) 407.
[16] A.B. Anderson, S.Y. Hong, J.L. Smialek, J. Phys. Chem. 91 (1987) 4251.
[17] A.J. Bridgeman, J. Rothery, J. Chem. Soc. Dalton Trans. 2 (2000) 211.
[18] J.F. Harrison, Chem. Rev. 100 (2000) 679.
[19] A. Kamariotis, T. Hayes, D. Bellert, P.J. Brucat, Chem. Phys. Lett. 316 (2000) 60.
[20] J. Sugar, C. Corliss, J. Phys. Chem. Ref. Data 14 (suppl) (1985) 2.
[21] R.W. Field, Ber. Bunsen-Ges. Phys. Chem. 86 (1982) 771.
[22] L.A. Kaledin, J.E. McCord, M.C. Heaven, J. Mol. Spectrosc 173 (1995) 499.
[23] S. Johansson, U. Litén, J. Sinzelle, J.-F. Wyart, Physica Scripta. 21 (1980) 40.
[24] M.J. Frisch et al, GAUSSIAN 98, Revision A.3, Gaussian, Inc., Pittsburgh, PA, 1998.
[25] M.N. Glukhovtsev, R.B. Bach, C.J. Nagel, J. Phys. Chem. A 101 (1997) 316.
[26] C.W. Bauschlicher Jr., P. Maitre, Theor. Chim. Acta. 90 (1995) 189.
[27] A. Kamariotis, T. Hayes, D. Bellert, P.J. Brucat, Chem. Phys. Lett. 316 (2000) 60.
[28] J. Lei, P.J. Dagdigian, J. Chem. Phys. 112 (2000) 10221.